Rarefied gas flows induced by temperature fields and their applications

京大・工・航空宇宙   杉元   宏 (Hiroshi Sugimoto)
Department of Aeronautics and Astronautics,
Graduate School of engineering,
Kyoto University

This paper consists of two parts. In the first part, we present the result of the numerical simulation on the steady gas flow in a pump driven by thermal edge flow, which is proposed in *Rarefied Gas Dynamics*, AIP, New York, 138–141 (2002). A new finding of this analysis is the possibility of the alternative design of the flow channel of the pump. According to the new design of the channel, a rarefied gas flow is induced through a pair of parallel wire meshes with different temperatures. In the second part of this paper, we confirm this phenomena by simple experiments.

1   Introduction

In a rarefied gas, where the mean free path of the gas molecule is not negligible compared with the scale of the system, the temperature field of the gas is deeply related to the gas motion. The flow of the rarefied gas is induced by the temperature fields of the gas even if there is no external force. The thermal transpiration flow [1,2], which is a flow induced in a pipe with a temperature gradient along it, is a well known example, and now it is known that various flows with different properties are induced by the temperature fields. [3] The thermal transpiration flow in a pipe suggests a possibility of a pump without moving parts. That is, if we connect two tanks of different temperatures by a thin pipe of a uniform cross section, the thermal transpiration flow is induced in the pipe and thus we can maintain a pressure difference between these tanks. However the difference of the pressure between the tanks is proportional to the temperature difference. Thus this simple idea is not practical since the variations of temperature of material is rather limited than that of pressure of the gas. In 1910, Knudsen carried out an experiment by a single pipe with periodic variations of diameter and temperature (Fig. 1), and succeeded to obtain the pressure ratio 10, which is fairly larger than the temperature ratio in the system. [4] Recently this type of pumps driven by temperature field attracts researchers again, since it does not require moving parts and has a possibility of the application as micro devices. [5–14]

The author and Sone have been carried out two experiments of the pumps driven by the flows induced by the temperature field. The first one is the pump driven by the thermal transpiration flow. [10] (This type of pump is called "Knudsen compressor" now.) The experiment showed that it can reduce the pressure of a tank of 8 liter to a half in 300 sec, but its energy efficiency is lower than standard commercial pump by far. This pump is very primitive and many improvements are required. One of the reason of the low efficiency of the Knudsen compressor is the temperature gradient of the pipe wall which is essential to the thermal transpiration flow. That is, a heat flux through a pipe wall, which is the loss of the energy, is required to maintain the temperature gradient. In order to reduce this loss of

the energy, we developed a new type of a pump [12] driven by the thermal edge flow [15,16]. (This type of pump may be called "thermal edge compressor".) The thermal edge flow is a localized flow induced around a sharp edge of heated (or cooled) plate (Fig. 2). It is induced by a sharp variation of the temperature of the gas around the edge of the plate, thus the temperature gradient of solid body is not required to induce the flow. Some energy will be lost through the gas around the heated body, but it will be smaller than that expected when we replace the gas by solid materials. Actually the energy efficiency of the thermal edge compressor in our experiment is about 6 times better than that of our Knudsen compressor in Ref. 10.

In order to devise these compressors, the information on the behavior of the gas in the channel of the pump is required. As for the Knudsen compressor, there are some amounts of works [6-9]. The corresponding analysis for the thermal edge compressor is recently published in Japanese [13]. In the present paper, the main results of the paper and the new results on the alternative design of the thermal edge compressor are presented in Sec. 3. The result on the alternative design is unique since it shows that a new type of rarefied gas flow is induced through a pair of parallel wire meshes with different temperature. In the next part of this paper, Sec. 4, the results of two preliminary experiments on the existence of the flow through a pair of wire meshes are reported.
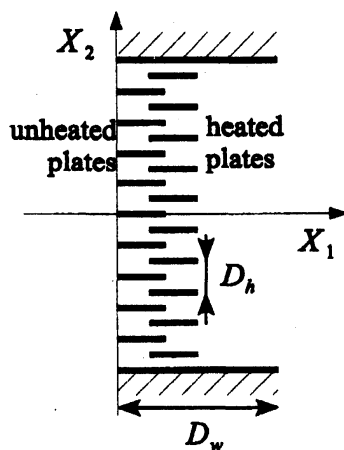
2 Thermal Edge Compressor

The thermal edge compressor consists of a number of driving units connected in series, as well as the Knudsen compressor. Figure 3 shows an 2D model of the unit of the thermal edge compressor devised in Ref. 12. The channel is equipped with a pair of two arrays of plates, one is heated (temperature T_h) and the other is unheated (temperature T_c). The size of the unit in X_1 direction D_w is larger than the total width of the set of arrays of the plates, thus some space is left around the set of arrays of the plates. The mechanism of this unit is as follows. In the overlapping region of the two arrays of plates, a temperature gradient in X_1 direction is induced. This temperature gradient induces the thermal edge flow in X_1 direction. In the gas region around other edges of each plate, the temperature of the gas is roughly uniform since there are lots of plates of identical temperature in X_2 direction in a space left around the array. Therefore the thermal edge flow induced there is weaker than those induced in the overlapping region. In the narrow regions between the plates of each array, the flow is not induced since the temperature of the gas is roughly
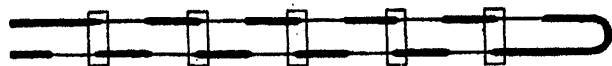
Fig. 1: The experimental apparatus by Knudsen (Ref. 4). The diameter of the thin part is 0.4mm and that of thicker part is 10mm, and the temperature difference between the heated part and unheated part is about 500K.
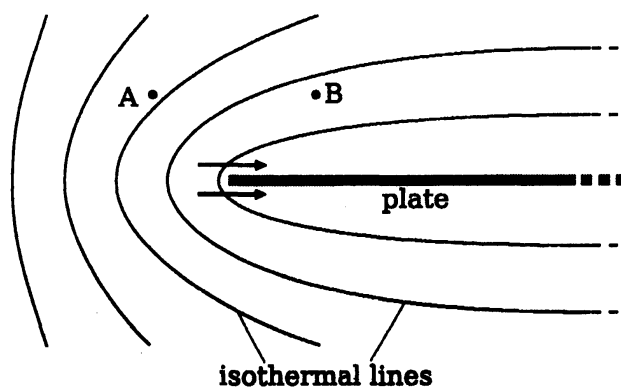
Fig. 2: Thermal edge flow. The points A and B are about one mean free path away from the edge of the plate. Near the edge, the isothermal lines are sharply curved, and thus the temperature is non-uniform along the plate. The molecules impinging on the edge region from the left side are roughly represented by those from A and the molecules from the right side by those from B, where the gas is hotter than at A when the plate is heated. The situation is similar to that over a non-uniformly heated plate, where the thermal creep flow [1] is induced. Thus, a flow is induced in the direction of the arrows around the edge of a heated plate.

Fig. 3: A unit of thermal edge compressor.

uniform there. In summary, the flow is mainly induced in the overlapping region between the heated array and unheated array. Thus this unit induces a gas flow in X_1 direction.

3 Numerical simulation

We carry out two cases of numerical simulation on the flows in the thermal edge compressor, following the numerical analysis on the gas flows in the Knudsen compressor in Refs. 6 and 7.

Problem-I: Investigate the maximum flow rate obtained by the thermal edge compressor. The maximum flow rate here is the flow rate obtained when the pressures of the gas at both ends of the compressor are identical, or there is no average pressure gradient along

the compressor system. For this purpose we consider a pump system where a infinitely many units of the thermal edge compressor are connected in series, and investigate the steady gas flows in the system assuming that the behavior of the gas is periodic along the system and the cycle is the length of the unit along the system.

Problem-II: Investigate the maximum compression ratio obtained by the thermal edge compressor. We are interested in the pressure difference between the both ends of the pump system that is required to cancel the driving gas flow described in *Problem-I*. In this case we consider a pump system where finite numbers of units are connected in series. Then we investigate the steady distribution of the pressure of the gas in the system when the both ends of the system are closed by the walls.

The shape of the flow channel of thermal edge compressor is rather complicated, thus there are many parameters on it. The purpose of this paper is not the optimization of these parameters, but to show the basic properties of the thermal edge compressor. Furthermore the results given in Sec. 3.3B will show that the design of the flow channel is not restricted to the one shown in Fig. 3. Therefore we first restrict ourselves to the channel shape shown in Fig. 3, and omit the explanation of detailed shape on it. We use only the following parameters of the compressor unit in this paper. T_h, T_c: the temperature of two arrays of plates (the temperature of side wall is also T_c); D_h: the distance between the plates in a array; n: the number of plates with temperature T_h (or the number of small flow channels of height D_h), D_w: the length of a unit in X_1 direction.

3.1 Basic Equation

The analysis is carried out on the basis of the Boltzmann equation for hard sphere molecules: [17]

$$\xi_1 \frac{\partial f}{\partial X_1} + \xi_2 \frac{\partial f}{\partial X_2} = J(f, f), \tag{1}$$

$$J(f, f) = \frac{d_m^2}{2m} \int_{|\xi_*|<\infty, |a|=1} [f(\xi'_*)g(\xi') - f(\xi_*)g(\xi)] |V \cdot a| d\Omega(a) d\xi_*, \tag{2}$$

$$\xi' = \xi + (V \cdot a) a, \quad \xi'_* = \xi_* - (V \cdot a) a, \quad V = \xi_* - \xi. \tag{3}$$

The notation is as follows. d_m: the diameter of a molecule; m: the mass of a molecule; ξ_i: the molecular velocity; f: velocity distribution function of gas molecules; $d\xi_* = d\xi_{*1} d\xi_{*2} d\xi_{*3}$; $d\Omega(a)$: solid angle element in the direction of unit vector a.

The boundary condition on solid walls is the diffuse reflection:

$$f(\xi \cdot n > 0) = \frac{\sigma_w}{(2\pi RT_w)^{3/2}} \exp\left(-\frac{|\xi|^2}{2RT_w}\right), \tag{4}$$

$$\sigma_w = -\left(\frac{2\pi}{RT_w}\right)^{1/2} \int_{\xi \cdot n < 0} \xi \cdot n f d\xi, \tag{5}$$

where T_w and n are, respectively, the temperature and the unit normal vector to the boundary, pointed to the gas. R is the specific gas constant ($R = k_B/m$, k_B: the Boltzmann constant). In the numerical simulation the specular reflection condition

$$f(\xi \cdot n > 0) = f(\xi - 2(\xi \cdot n)n), \qquad (6)$$

is also used to represent a symmetric surface.

The macroscopic quantities are defined by the moments of the velocity distribution function f as follows:

$$\rho = \int f d\xi, \qquad v = \frac{1}{\rho} \int \xi f d\xi, \qquad T = \frac{1}{3R\rho} \int |\xi - v|^2 f d\xi, \qquad p = R\rho T, \qquad (7)$$

where ρ, v, T, and p are the density, flow velocity, temperature and pressure of the gas, respectively. The integrations are carried out over the whole space of ξ.

An important length of scale in the Boltzmann equation is the mean free path of the gas molecule. For hard sphere molecules, its size at equilibrium state at rest depends on d_m, m, and density of the gas. Thus we define the reference mean free path ℓ_{av} by using the average density over a period (*Problem-I*), or average density over the pump system (*Problem-II*). That is,

$$\ell_{av} = m/(\sqrt{2}\pi d_m^2 \rho_{av}). \qquad (8)$$

The Knudsen number Kn is defined by

$$\mathrm{Kn} = \ell_{av}/D_h. \qquad (9)$$

For the convenience of the description we introduce reference pressure p_0 by

$$p_0 = R\rho_{av}T_c. \qquad (10)$$

3.2 Method of solution

The system of equation (1)-(6) is analyzed numerically by the Direct Simulation Monte Carlo (DSMC) method [18], where the gas molecules are replaced by a numbers of simulation particles, and the behavior of the particles over a small time step is simulated by two separate processes, the process of motion of the particles without collisions and the process of changing their velocities by collisions between particles. Thus the method is time-dependent. We obtained the steady solution of *Problem-I* or *Problem-II* by chasing a long time behavior of the results. The DSMC method is widely used in the studies of rarefied gas flows, and the numerical procedure used here is just the same as the one described in Ref. 6. What is special in this paper is only that the shape of the flow field is rather complicated by many pieces of plates. The DSMC method is convenient for this type of the problems since we can divide the flow field into many small rectangular domains by introducing virtual boundaries in the gas region. We carry out the numerical simulation in each rectangular domain by using additional boundary conditions on the virtual boundaries that the molecules which disappear into the virtual boundary revive
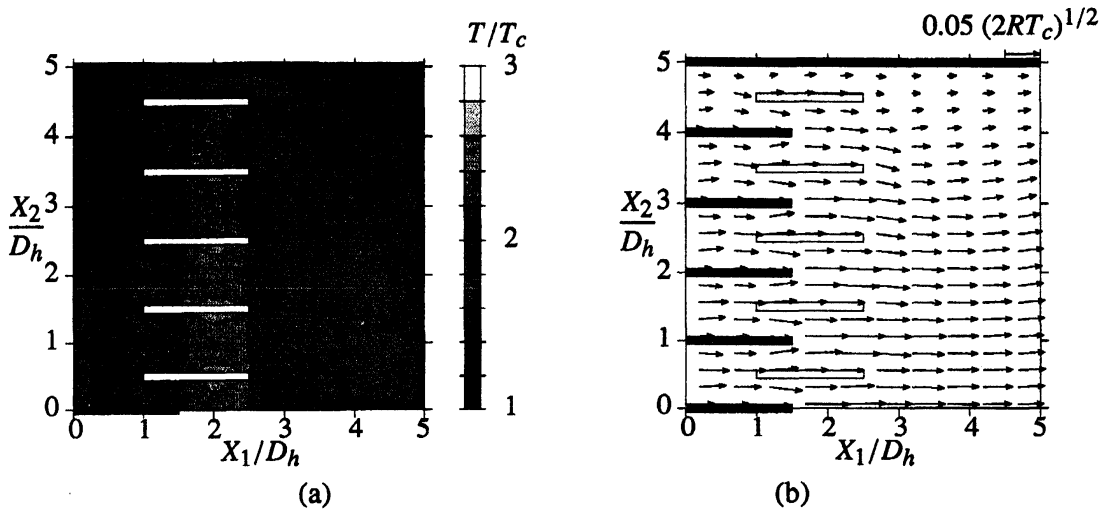
Fig. 4: One way flow in the thermal edge compressor I (Problem I). $T_h/T_c = 3, n = 10$, and $Kn = 1$. (a) Temperature field and (b): flow velocity field. The temperature field in (a) is shown by the shade of the darkness, and its scale is shown in the right end of the panel. The arrows in (b) indicate the flow velocity at their starting points, whose scale is shown on the right shoulder of the panel.

from the virtual boundary of corresponding adjacent domain. This method is also effective for parallel computers since we can carry out the simulation for each domain almost independently except small amount of information on the molecules that pass the virtual boundaries in each time step of numerical simulation.

3.3 Results

A One way flow for basic channel

Here we explain the result for *Problem-I*, the maximum flow rate obtained by the thermal edge compressor. Figure 4 shows the temperature and flow velocity fields for the case of $T_h/T_c = 3$, $Kn = 1$, and $n = 10$. Only the part $X_2 > 0$ is analyzed since the system is symmetric with respect to $X_2 = 0$, and the cyclic boundary condition is applied to $X_1 = 0$ and $5D_h$. The temperature gradient is large in the gas at the overlapping region of two arrays of plates ($D_h \lesssim X_1 \lesssim 1.5D_h$). On the other hand, the temperature gradient is small around the other ends of plates ($X_1 \sim 0, 2.5D_h$ or $5D_h$). As the result, the one-way flow is induced in X_1 direction. The flow speed v_1 decreases near the side wall at $X_2 = 5D_h$. This is because of the temperature between the side wall and the nearest plate (the plate at $X_2 = 4.5D_h$) is roughly symmetric with respect to X_1 direction, and only a small size of net flow v_1 is induced there.

Figure 5 shows the one-way flow for the case of $T_h/T_c = 3$, $Kn = 1$, and $n = 40$. The effect of side wall at $X_2 = nD_h/2$ is confined in several small channels (or several D_h in X_2 direction) near the side wall, and a periodic structure of the flow field in X_2 direction is seen around the centerline of compressor unit ($X_2 \sim 0$).
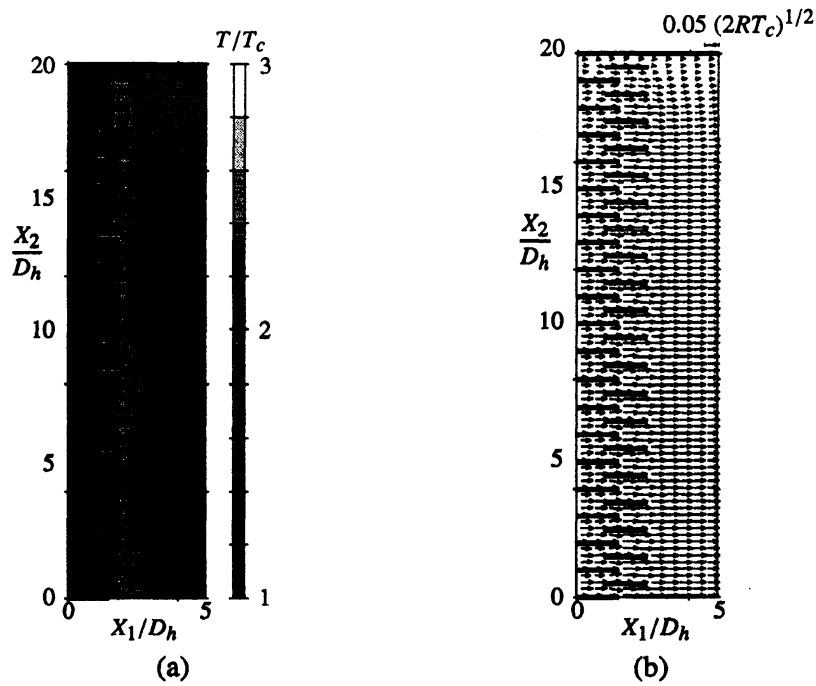
Fig. 5: One way flow in the thermal edge compressor II (*Problem I*). $T_h/T_c = 3, n = 40$, and $Kn = 1$. (a) Temperature field and (b): flow velocity field. (See the caption of Fig. 4).
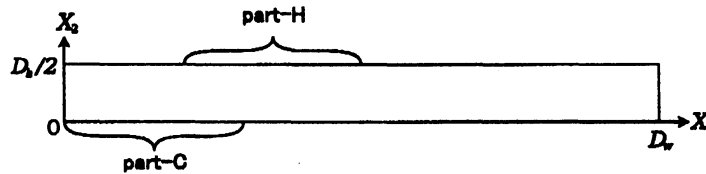
Fig. 6: A simpler model of a unit of the thermal edge compressor. $X_2 = 0$ and $D_h/2$ are the symmetric surface. The part-C represents the unheated plate, and part-H does the heated wall.

This result leads a simplified model of the thermal edge compressor depicted in Fig. 6. Consider a rectangular domain $0 < X_1 < D_w$ and $0 < X_2 < D_h/2$. The boundary condition at a part of the lower boundary $X_2 = 0$ (say, part-C in Fig. 6) is the diffuse reflection (4) at temperature T_c, and a part of the upper boundary $X_2 = D_h/2$ (part-H in Fig. 6) is the diffuse reflection at temperature T_h. The boundary condition at other part of upper and lower boundary is the specular reflection (6). The condition for boundaries normal to X_1 direction will be defined depending on the purpose of the problems; In this section (*Problem-I*), we apply the cyclic boundary condition. This model is denoted by $n \rightarrow \infty$ for the convenience of expression.

The result for mass flow rate for $T_h/T_c = 3$ is shown in Fig. 7. In the figure, the mass
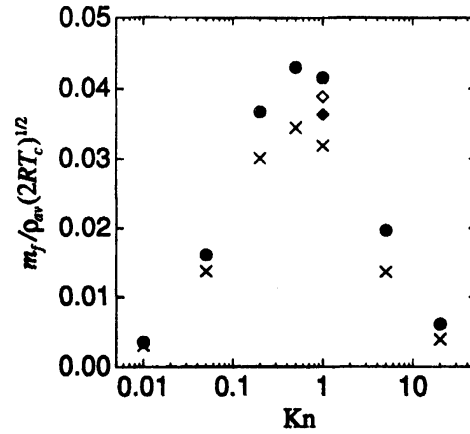
Fig. 7: Nondimensional mass flow rate per cross sectional area $m_f/\rho_{av}(2RT_c)^{1/2}$ vs Knudsen number Kn of the thermal edge pump (*Problem-I*). $T_h/T_c = 3$. ✕: $n = 10$, ◆: $n = 20$, ◇: $n = 40$, ●: $n \to \infty$.

flux per unit time and per unit area of the cross section of the compressor unit

$$
m_f = \begin{cases}
\dfrac{2}{nD_h} \displaystyle\int_0^{nD_h/2} \rho v_1 dX_2 & (n < \infty), \\[3mm]
\dfrac{2}{D_h} \displaystyle\int_0^{D_h/2} \rho v_1 dX_2 1 & (n \to \infty),
\end{cases}
\tag{11}
$$

are plotted for Knudsen number Kn =0.01, 0.5, 0.2, 0.5, 1, 5, and 10 for $n = 10$ and ∞, and Kn = 1 for $n = 20$ and 40. The nondimensional mass flux $m_f/\rho_0(2RT_c)^{1/2}$ takes its maximum value around Kn ~ 0.5, and it decreases as Kn → 0 or ∞. The effect of the side wall is clearly seen in the cases for $n = 10$, 20, 40, and ∞ at Kn = 1. The mass flux approaches to that for $n \to \infty$ as n increases and the deviation of m_f from the case of $n \to \infty$ is roughly proportional to $1/n$. This supports the previous discussion that the effect of side wall is confined in a small region near the side wall.

B Alternative design of flow channel

The preceding result shows that the velocity of the one-way flow (which is roughly represented by m_f/ρ_{av}) in the thermal edge compressor takes its maximum value when the scale of the small flow channel (D_h) is comparable to the mean free path ℓ_{av} of the gas molecules. The ℓ_{av} at high pressure is, however, quite small [cf. Eq. (8). $\ell_{av} \sim 0.07\mu$m under the atmospheric pressure and the standard temperature], and it can be difficult to realize a complicated flow channels by the usual engineering process. Here we investigate the possibility of alternative design of flow channel of the thermal edge compressor.

In the following numerical analysis, we arrange objects of various shape in the flow channel, and the gas region is not represented only by $X_1 = Const$ or $X_2 = Const$. In this paper such shapes of gas region is also approximately represented by the union of many rectangular domains as is explained in Sec. 3.2. This simple strategy may lead the

increase of computational time, since, in some cases, we have to prepare large number of rectangular regions to represent the shape of the boundary. Therefore we carry out the numerical simulation only for the limiting case for many small flow channels ($n \to \infty$ in Sec. A).

Some of the results are shown in Fig. 8. In the figures, the temperature field is shown by the shade of the darkness and flow velocity is represented by arrows. In the case of Fig. 8(a), two squares with one side ℓ_{av} in length are put in the channel. The temperature of square at smaller X_1 is T_c, and that of larger X_1 is T_h. In this case the temperature field around each square is slightly asymmetric with respect to X_1 direction, and one-way flow is induced in X_1 direction. The mass flux m_f per unit area of the cross section of the compressor unit[1] is $m_f/\rho_{av}(2RT_c)^{1/2} = 0.0032$. The mass flux m_f increases if we round off the edges of these squares. In the case of Fig. 8(b), the radius of the curvature is $\ell_{av}/4$ and $m_f/\rho_0(2RT_c)^{1/2} = 0.0043$. In Fig. 8(c), the object is cylinder with radius $\ell_{av}/2$, and $m_f/\rho_0(2RT_c)^{1/2} = 0.0053$.

In Fig. 8(c), the objects put in the channel are the circular cylinders, and thus there is no "sharp edge" of a solid body which is usually required to induce the thermal edge flow. Of course there is no thermal edge flow around a circular cylinder put isolated from other boundaries. In the case of Fig. 8(c), we are considering the behavior of the gas in a compressor unit which consists of two parallel meshes with different temperatures, since the boundaries $X_2 = 0$ and $D_h/2$ are the symmetric surface. These two meshes induce a temperature gradient of the gas in X_1 direction between these meshes. This temperature gradient induces a one way flow similar to those seen in the thermal edge compressor, because the size of the wires and distance between the meshes are of the order of the mean free path of the gas molecules ℓ_{av} (= $D_h/2$ in Fig. 8).

As is discussed in Sec. A, the width of the small channel of the thermal edge compressor would be of the order of the mean free path of the gas molecules ℓ_{av}. From the result in this section, it is possible to infer that one-way flows are induced by any object with a radius of curvature of the order of ℓ_{av}. These two informations means that one can use various porous materials with pole size of ℓ_{av} to construct the thermal edge compressor unit. From the view point of engineering, it is important result which enables the thermal edge compressors with micro channels works at higher pressure of gases.

C Pump effect

Next we consider *Problem-II*, the steady pressure distribution in a pump system consisting of a number of compressor units connected in series with their two ends of the pump system being closed by the walls. The number of the compressor units N is limited in the DSMC simulation. The accuracy and computational speed of DSMC depend on the number density of simulation particles, which show unbalanced distribution as N increases in this problem. This results in the low accuracy at low density regions and a low

---

[1]A modification of the domain of integration in the definition of m_f in (11) is required since some part of the domain of integration can be inside the solid body. The integration here is carried out only in the gas region.
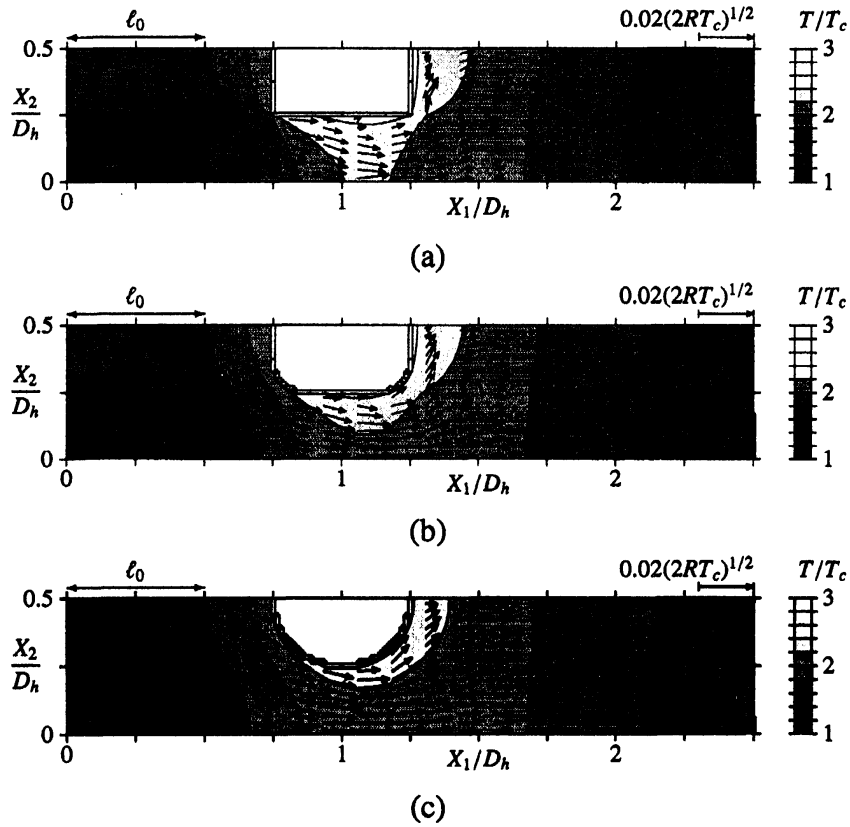
Fig. 8: One way flow in the thermal edge compressor III (*Problem I*). $T_h/T_c = 3$. (a) The case where the plates are replaced with square boxes with temperature T_c (shown by a dark box) and T_h (shown by blight box); (b) The case with square boxes with the round off (the radius of the curvature is $D_h/4$); and (c) The case with a cylinder with diameter $D_h/2$. (See the caption of Fig. 4.) The size of the reference mean free path ℓ_{av} is shown on the left shoulder of each panel.

computational speed at high density regions. In Ref. 6, it is shown that the compression ratio of a compressor unit is a function of the local Knudsen number Kn_L defined by the average density of the gas in each unit in the system, and their relation is determined as follows: (i) Carry out the numerical simulation with $N = 10$ for Knudsen number Kn defined by the density ρ_{av} of the gas averaged over whole pump system; (ii) Obtain a part of the relation between the compression ratio and Kn_L from the result of (i); (iii) Repeat (i) and (ii) for various Kn. In this paper, we follow this method. We also consider a pump system of 10 compressor units of basic type shown in Figs. 3 or 6, and the both ends of the pump system are closed by the walls with temperature T_c. We first define the pressure averaged over the cross section of the pump $p(X_1)$ by

$$\bar{p}(X_1) = \begin{cases} \dfrac{2}{nD_h} \displaystyle\int_0^{nD_h/2} p\, dX_2 & (n < \infty), \\[2ex] \dfrac{2}{D_h} \displaystyle\int_0^{D_h/2} p\, dX_2 & (n \to \infty). \end{cases} \tag{12}$$
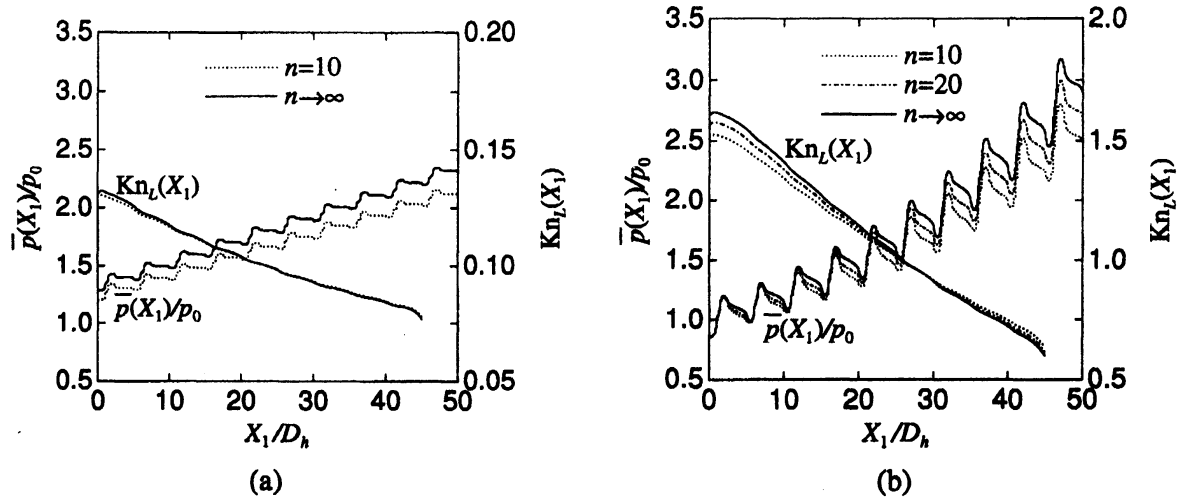
Fig. 9: The distribution of the average pressure $\bar{p}(X_1)$ and local Knudsen number $\mathrm{Kn}_L(X_1)$ in the steady state of a closed system of 10 compressor units (Problem II). $T_h/T_c = 3$. ⋯⋯⋯: $n = 10$, — · —: $n = 20$, ——: $n \to \infty$. (a) Kn=0.1, (b) Kn=1.
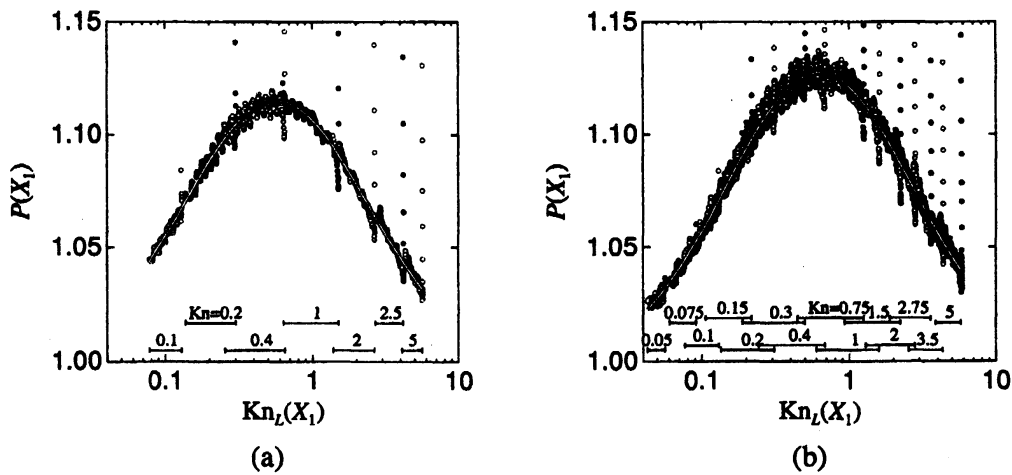
Fig. 10: The compression ratio of a compressor unit $P(X_1)$ vs the local Knudsen number $\mathrm{Kn}_L(X_1)$ (*Problem II*). $T_h/T_c = 3$. (a) $n = 10$, $\bigcirc$: Kn $= 0.1, 0.4, 2, 5$; ●: $0.2, 1, 3.5$. (b) $n \to \infty$, $\bigcirc$: Kn $= 0.05, 0.1, 0.3, 0.75, 1.5, 2.75, 4$; ●: $0.075, 0.2, 0.4, 1, 2, 3.5$. The ranges of local Knudsen number $\mathrm{Kn}_L(X_1)$ for each value of Kn are shown in the bottom of the figure. The white line represents the approximation curve Eq. (15).

The compression ratio $P(X_1)$ of a compressor unit between X_1 and $X_1 + D_w$ is defined by
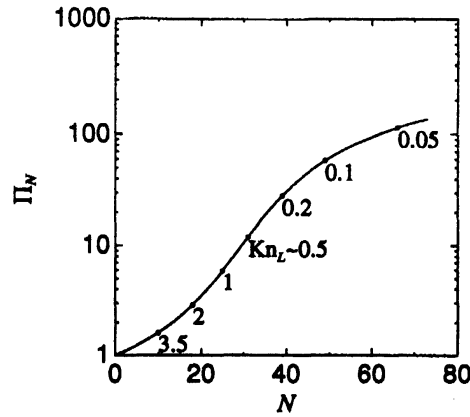
$$P(X_1) = \bar{p}(X_1 + D_w)/\bar{p}(X_1),\qquad(13)$$

and the local Knudsen number $\mathrm{Kn}_L(X_1)$ by

$$\mathrm{Kn}_L(X_1) = \frac{m}{\sqrt{2}\pi d_m^2\, \bar{p}(X_1)D_h} = \frac{\rho_{av}}{\bar{p}(X_1)}\mathrm{Kn},\qquad(14)$$

where $\bar{p}(X_1)$ is the average density between X_1 and $X_1 + D_w$.

The examples of the distribution of the average pressure $\bar{p}(X_1)$ and the local Knudsen number $\mathrm{Kn}_L(X_1)$ for the case $T_h/T_c = 3$, Kn = 0.1 and 1 are shown in Fig. 9. The average

Fig. 11: The compression ratio Π_N obtained by N compressor units (*Problem II*). $T_h/T_c = 3, n \to \infty$, $\text{Kn}_{L(1)} = 5.7$. The marks ● show the points (i, Π_i) where $\text{Kn}_{L(i)} \sim 0.05, 0.1, 0.2, 0.5, 1, 2, 3.5$.

pressure $\bar{p}(X_1)$ increases showing some vibrations as X_1 increases. The profile of local Knudsen number $\text{Kn}_L(X_1)$ is smoother than that of $\bar{p}(X_1)$. It is because Kn_L is defined by the average density over a unit length D_w and $\bar{p}(X_1)$ by the values at a cross section at X_1. The profile of Kn_L shows local variations at both ends of the pump system. This corresponds to the effect of end walls of the pump system which is also seen in Ref. 6.

The sets of $(\text{Kn}_L(X_1), P(X_1))$ for various Knudsen numbers Kn are plotted in $\text{Kn}_L - P$ plane for the case $T_h/T_c = 3$ and $n = 10$ and ∞ in Fig. 10. The points (Kn_L, P) form a curve $P'(\text{Kn}_L)$ in the $\text{Kn}_L - P$ plane. The data for X_1 near the ends of the pump system deviate from the above curve $P'(\text{Kn}_L)$ due to the effect of the end walls of the system. An approximation of $P'(\text{Kn}_L)$:

$$P'(x) \sim \exp\left[C_0 + C_1 \ln x + C_2(\ln x)^2\right] + 1, \quad C_i : \text{Constant}, \tag{15}$$

is also shown in the figure, where C_i are determined by the least square method from the data (Kn_L, P) except those close to the ends of the pump system. The values of C_i are $(C_0, C_1, C_2) = (-2.24, -0.276, -0.244)$ for $n = 10$ and $(-2.11, -0.221, -0.238)$ for $n \to \infty$.

The compression ratio Π_N of a pump system consists of N units can be estimated by using Eq. (15). That is, we estimate the local Knudsen number $\text{Kn}_{L(i)}$ of i-th unit and the total compression ratio of the system Π_N from a initial local Knudsen number at i-th unit by

$$\text{Kn}_{L(i+1)} = \text{Kn}_{L(i)}/P'(\text{Kn}_{L(i)}), \quad \Pi_N = \prod_{i=1}^{N} P'(\text{Kn}_{L(i)}). \tag{16}$$

An example of the result is shown in Fig. 11, for the case of $T_h/T_c = 3$ and $n \to \infty$ with initial local Knudsen number $\text{Kn}_{L(1)} = 5.7$.

(a)   (b)   (c)
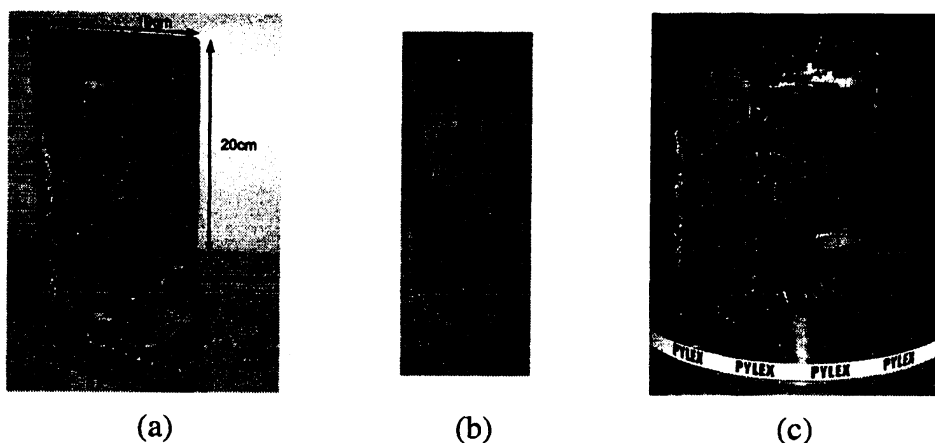
Fig. 12: The device that forms a flow channel of the scale of 1mm. (a) Unheated part. It is a rectangular copper plate (thickness 1mm) of 200mm in height and 200mm in width. There is a rectangular hole of 80mm in width and 100mm in height. A large number of copper wires with diameter 1mm is attached in the horizontal direction to the hole with the solder. (b) Heated part. An aluminum frame forms a square flow channel of side 100mm in length. A large number of Kanthal heater wires with diameter 1mm in vertical direction are attached by alumina adhesive on one side of the frame. (c) The assembled device. The wires around the heated part supply the electric current to the heater wire.
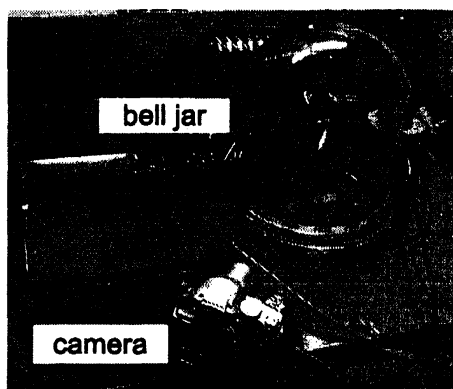
4 Experiment

In the course of the numerical simulation in Sec. 3, a one-way flow under the condition of periodic flow along the pump system (*Problem-I*) is induced by the newly designed unit, which consists of a pair of parallel wire meshes with different temperatures. It means that there will be a rarefied gas flow through a pair of parallel wire meshes with different temperatures. The flow is, however, not found in literature. Therefore, we will carry out a preliminary experiment in this section to observe this phenomena in a rarefied gas.

4.1 Experiment on the channel width of 1mm

A   Experimental apparatus

Here we present the setup for the experiment of the channel width of 1mm. The device consists of two parts: one is the unheated part, and the other is the heated part. The former is a rectangular copper plate (thickness 1mm) of 200mm in height and 190mm in width. This plate has a hole of 100 mm in height and 80mm in width [Fig. 12(a)], and many copper wires with diameter 1mm in horizontal direction are arranged in the hole. The latter is a aluminum frame [Fig. 12(b)] which forms a square flow channel of side 100mm in length, and many Kanthal heater wires with diameter 1mm in vertical direction are attached by alumina adhesive. The gap between each of these wires, copper and Khantal, is about 1mm.

The aluminum frame is hung on the copper plate by several Nylon support parts so that the side of the mesh of heater wire face to the wire mesh on the copper plate. The dis-

Fig. 13: The overview of the experimental apparatus. The device is set inside the glass bell jar. The motion of the film or windmill is observed by the camera positioned appropriately.

(a)   (b)
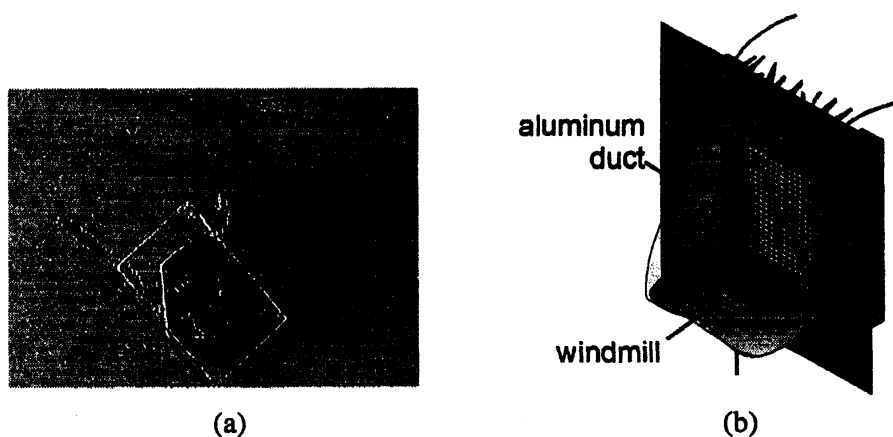
Fig. 14: (a) Windmill to detect the vertical gas flow. The vane is made of mica. The vane is supported by a bearing of tiny glass cup and a steel needle. (b) The aluminum duct and a hole for the windmill, attached to the unheated side of the device. The windmill detects upward flow if a gas flows through the device from unheated side to heated side.

tance between these wire meshes is kept as close as possible, while there is a small space between them. (We can detect the contact between them by measuring the electric resistance.) Then the whole system is put in a glass bell jar, whose inner pressure is controlled from the atmospheric pressure (1.01×10^5 Pa) down to about 0.5 Pa by external oil-sealed vacuum pump (Fig. 13). The copper plate of the unheated part is connected to the steel base of the vacuum chamber to keep the temperature close to the room temperature.

We supply the electric current to the heater wire with the gas pressure p in the bell jar being kept at some constant value. Then the gas flow through this pair of wires are detected by two separate experiments: (A) A thin aluminum film (thickness 4μm) of width 60mm and height 80mm is hung on the flow channel in the side of the heated wire. We observe the motion of the film by a camera (Fig. 13); (B) Prepare a windmill which detects a flow in the vertical direction[Fig. 14(a)]. The windmill is set in an aluminum duct attached to the hole of unheated copper plate in the opposite side of the heated mesh as shown in Fig. 14(b). Each of experiments (A) and (B) is carried out more than 2 hours
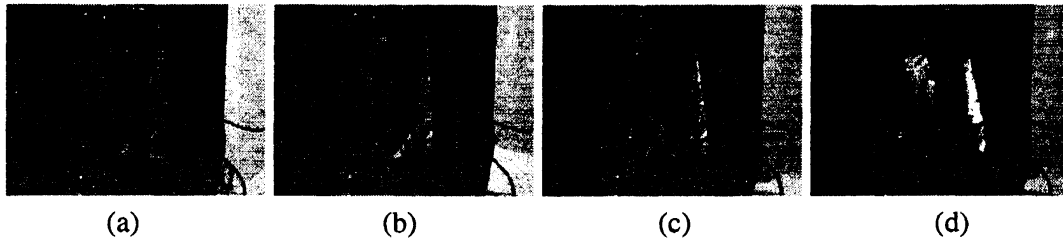
Fig. 15: The movement of the film in experiment (A) for the case of channel width of 1mm. I: The results for constant pressure $p=1$Pa and various energy supply E to the heater. (a) $E = 0$W, (b) 5.2W, (c) 12W, and (d) 21W.

after the heater is put on in order to wait the steady temperature of the device.
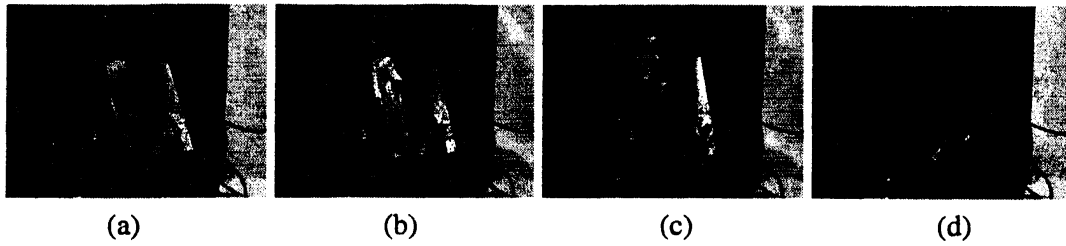
B Results

Two series of experiments are carried out for experiment (A). In the first series we observe the film for various energy to the heater $E = 0$, 5.2, 12, and 21W with keeping constant gas pressure $p = 1$Pa. The result is shown in Fig. 15. The film is gradually inclined as the energy E to the heater increases, and keeps at some angle as long as E and p are kept at constant value. The temperatures of the frame of the heated part and that of the copper plate of the unheated part are measured in a separate experiment. The temperature difference between them is 0.0K at $E = 0$W, 6.6K at 2.0W, 11.4K at 4.0W, and 19.8K at 8.5W. In the second series the energy to the heater E is fixed to 21W, and the observation is carried out for various p in the range from 1Pa to 2000Pa. Some of the results are shown in Fig. 16. The movement of the film takes maximum value at around 5Pa, where the mean free path of the air is about 1mm. The movement of the film vanishes as pressure increases. In this preliminary experiment it is difficult to conclude that this shows that the flow vanishes as Knudsen number decreases; We will discuss about the problem later in Sec. 4.3.

The experiment (B) is carried out for the case with $(E, p) = (0$W, 5Pa$)$, $(2$W, 5Pa$)$, $(18$W, 5Pa$)$, $(18$W, 20Pa$)$, and $(18$W, 100Pa$)$. There is no rotation of the windmill for the case of $(0$W, 5Pa$)$ or $(18$W, 100Pa$)$. For other cases, the windmill rotates and the direction of the rotation shows that the gas flow is upward. From the position of the windmill shown in Fig. 14(b), it means that the gas flows through the pair of wire meshes from unheated wire mesh to heated wire mesh. The rotation speed of the windmill is 95rpm at $(2$W, 5Pa$)$, 667rpm at $(18$W, 5Pa$)$, and 176rpm at $(18$W, 20Pa$)$.

4.2 Experiment on the channel width of 100μm

A Experimental apparatus

In order to confirm the applicability of the flows induced through the wire meshes to higher pressure, we carried out another experiment by using a stainless wire mesh which
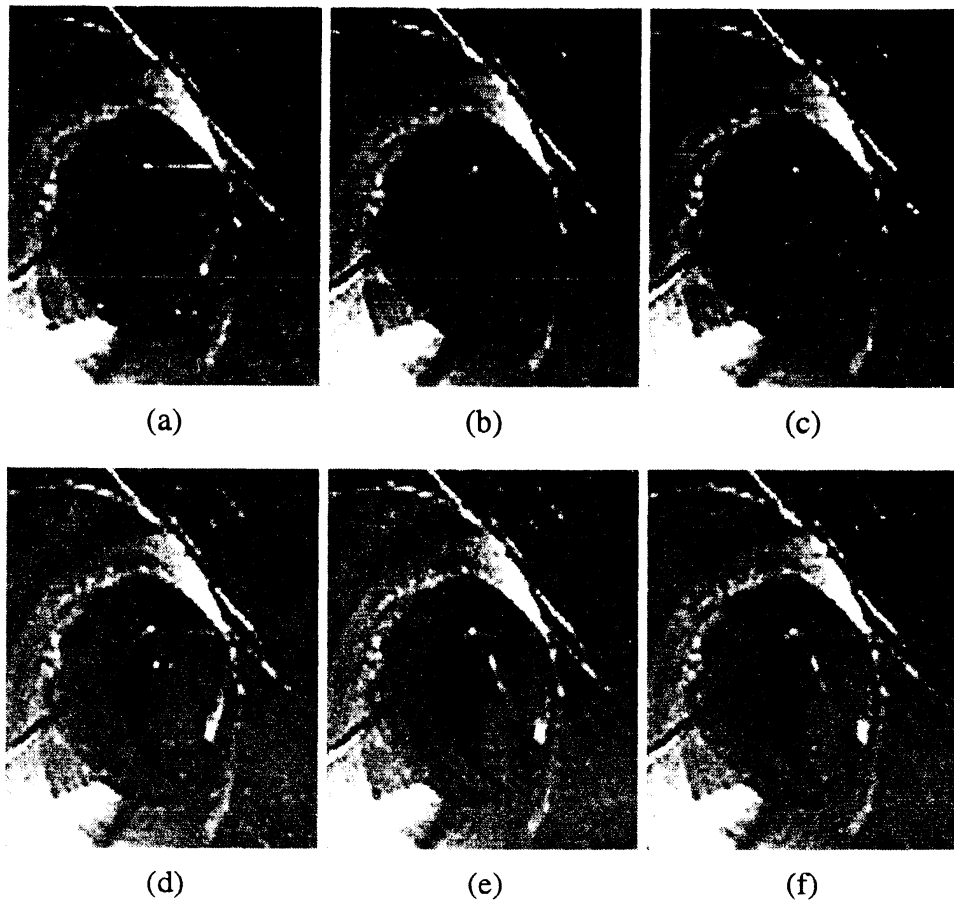
Fig. 16: The movement of the film in experiment (A) for the case of channel width of 1mm. II: The results for constant energy supply E=21W and various pressure p in the bell jar. (a) p =5Pa, (b) 10Pa, (c) 20Pa, and (d) 90Pa.
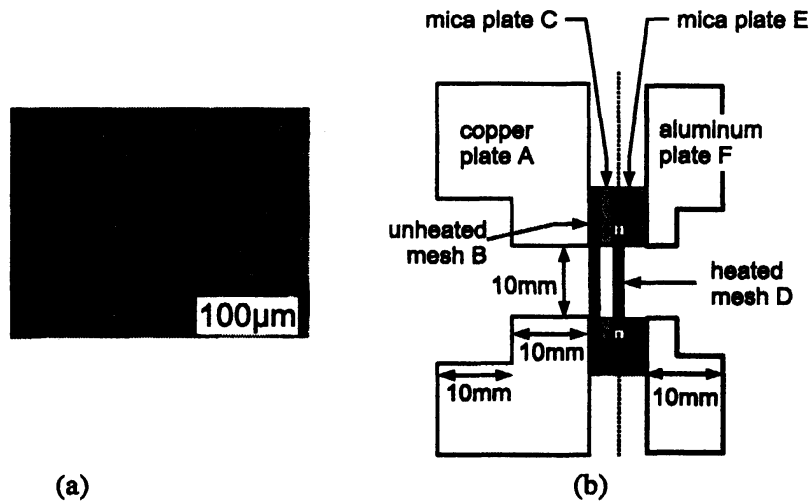
Fig. 17: Experimental setup for the experiment of flow channel of 100μm in width. (a) The stainless mesh. The scale of 100μm is shown at the right bottom corner of the figure. (b) The schematic figure (not to scale) of the device for the experiment. This figure shows the cross section along the flow channel to explain the layered structure of the device.

mesh size is about 100μm [Fig. 17(a)]. In this case we have to support two wire meshes with different temperatures in a small distance. For this purpose we constructed a layered structure as shown in Fig. 17(b). The base is a copper plate A (thickness 20mm) with a circular hole which is one end of the flow channel [Fig. 17(b)]. The diameter of the hole is 10mm on one side and it is enlarged to 20mm on the other side. This plate is connected to a bigger copper base which is connected to the steel base of a vacuum chamber to keep the temperature close to the room temperature [the copper base is omitted in Fig. 17(b)]. In order to support two wire meshes, the following material is layered on this copper plate: (i) A stainless wire mesh B. (ii) Several mica plates C (thickness 20μm), which forms a space around the hole of the copper plate A. (iii) Another stainless wire mesh D, to which two of electrical leads, shown by a dotted lines in Fig. 17(b), are attached to supply an electric current to the mesh. (iv) A mica plate E (thickness 2000μm). (v) A aluminum plate F (thickness 10mm) with a hole whose size is similar to that on copper plate A. The main purpose of mica plates C is to keep a space between the heated wire mesh B and the unheated wire mesh D. Another purpose of mica plates C is to maintain

(a)   (b)   (c)

(d)   (e)   (f)

Fig. 18: The movement of the film for the case of the channel width of $100\mu m$. The results for constant energy supply $E=1.5$W and various pressure p in the bell jar. (a) p =5Pa, (b) 20Pa, (c) 40Pa, (d) 100Pa, (e) 600Pa, and (f) 1000Pa.

the electrical insulation between them. The electrical insulation is required to prevent the electric current through wire mesh D from heating the wire mesh B. The mica plate E is also inserted to keep the electrical isolation between mesh D and plate F.

These layers are fastened tightly by several bolts, and the electrical isolation (including the space between meshes B and D) is confirmed by measuring the electrical resistance between mesh B and other metallic materials. Then the hole system is put in the same vacuum chamber as in section 4.1. In this system, the flow is detected by the movement of a thin film of mica or aluminum hung in the hole of the aluminum plate F.

B   Results

We supply the electric current to a wire mesh (mesh D in Fig. 17) and observe the tilting of the film. Two series of experiments are carried out; The first one is the case for various energy supply E =0, 0.06, 0.23, and 0.53W for p =10Pa, and the second is the case for various pressure p = 5,10,20,40,100,600, and 1000Pa for a fixed energy supply E =1.5W. In any case the film is constant if E and p are kept constant. Some of the results for

the second series are shown in Fig. 18. Compared with the previous experiment with the channel width of 1mm, the movement of the film is observed at slightly higher pressure; it takes maximum value at around p =20~40Pa. Incidentally the mean free path of air is about 200μm around p = 40Pa.

4.3 Discussion

In this section, we carried out two simple experiments to confirm the flow of a rarefied gas induced through a pair of parallel wire meshes with different temperatures. The movement of the thin film or the rotation of the windmill put in the channel of the flow shows that a flow is induced from the colder side to hotter side, and these phenomena is seen only in the rarefied gas regime. This flow is attributed to the flow induced by the temperature difference of two wire meshes. These experiments, however, are preliminary ones, and there should be several discussions on the results.

A point in question of the experiments given in this section is that the energy supply to the heater E is kept constant in the experiments for different pressure of the gas p. This will give some effect on the pressure dependence of the flow obtained by these experiments. The temperature of heated wire is determined by the given energy supply E and the loss of the energy. The loss consists of the radiation and heat flow through the support parts of the heated wire mesh and the loss of the energy carried by the gas molecules. The later energy loss is roughly proportional to p and the temperature difference between the wire meshes. Therefore, in these experiments, the temperature difference between the wire meshes decreases as p increases. (At the same time the temperature of the unheated wire mesh increases because the heat conduction between the unheated wire mesh and external environment is rather limited in a vacuum chamber.) Thus in these experiments, the flow through the pair of wire meshes may vanish in higher pressures by following two reasons: (1) the gas flow induced by rarefied effect vanishes since the mean free path becomes smaller; (2) the temperature difference between two wire meshes vanishes. Thus the dependence of the strength of the flow on pressure p is not clear by these experiments. The difficulty will be solved by the experiments with the temperature difference between two wire meshes being kept constant. It is possible for the system given in Sec. 4.1, and the result will be reported in the future work. In the system given in Sec. 4.2, it is difficult to measure the temperature of wire meshes since the wires are thin and total size of the heated area is rather small. A more sophisticated version of the device may be required to obtain the pressure dependence of the gas flow.

In the results for lower pressure, the motions of the film show that the effect of the flow decreases as the pressure decreases. This is because the gas molecule that arrives to the surface of wire experiences last molecular collision in the gas far from the pair of meshes, where the temperature of the gas is close to the room temperature.

We have to examine what we observe with the tilting of the film in these experiments. The weight of the aluminum film per unit area used in Sec. 4.1 is about 0.01kg/m^2, and the force required to support this film is about 0.1Pa per unit area. This force is supplied

by the momentum transfer through the flow channel per unit time. The momentum transfer (per unit area and per unit time) through a channel cross section consists of two parts, the contribution of the momentum carried by the gas motion (ρv_1^2) and the contribution of the stress. In the experiments shown in this section, the density of the gas is very small ($\rho \sim 10^{-5}$kg/m^3 at $p = 1$Pa). Therefore, it is impossible to support the film only by the contribution of ρv_1^2, since the flow speed may not be so large by the temperature difference given in these experiment. The contribution of the stress or pressure is important. That is, the motion of the gas in the flow channel is blocked by the film, and it induces pressure difference between both sides of the film. There is no analytical information on the pressure difference obtained by blocking the gas flow induced through wire meshes with different temperature. Instead, we estimate the pressure gradient obtained by blocking the thermal transpiration flow between two parallel plates with a temperature gradient dT/dX. According to the result of linearized Boltzmann equation, the mass flux through the two parallel plates is proportional to

$$\left(\frac{1}{p_0}\frac{dp}{dX}\right) M_P(\text{Kn}) + \left(\frac{1}{T_0}\frac{dT}{dX}\right) M_T(\text{Kn}),$$

where p_0, T_0 are the reference pressure and temperature, respectively.[17] Then we can obtain the relation between the pressure and temperature differences Δp and ΔT in some range of X when there is no mass flux, by using the numerical values for M_P and M_T. For example, $\Delta p \sim 0.3 p_0 \Delta T / T_0$ (Kn = 1) for hard sphere molecules, which is, for example, 0.1Pa when $p_0 = 5$Pa and $\Delta T / T_0 = 0.07$.

5 Concluding Remarks

In this paper, we carried out the numerical simulation of the rarefied gas flows in the thermal edge compressor, and clarified the maximum mass flow (*Problem-I* in Sec. 3) and pressure ratio (*Problem-II* in Sec. 3). In the course of the analysis we also tried to develop the alternative design of the thermal edge compressor adequate to high pressure range or compressor for micro channels, and it is shown that there is a wide variety of the design of the compressor. The result on the alternative design of the unit is also important as the fundamental study of the rarefied gas flows induced by the temperature fields, since it shows the presence of a rarefied gas flow through a pair of wire meshes with different temperatures. The flow, a new type of the flow which is not pointed out before, is demonstrated by simple experiments in Sec. 4. The experiment succeeded in showing that the flow is actually induced, but its dependence on the gas pressure or the Knudsen number is not still clear by these preliminary experiments.

Acknowledgment

References

[1] J. C. Maxwell: *Philos. Trans. Roy. Soc. London* **170** (1879) 231–256.

[2] T. Takaishi and Y. Sensui, *Trans. Faraday. Soc.* **59** 2503 (1963).

[3] Y. Sone: in *Annual Review of Fluid Mechanics*, (Annual Reviews, Palo Alto, 2000) **32**, 779–811.

[4] M. Knudsen: *Ann. Phys. (Leipzig)* **31** (1910) 205–229.

[5] G. Pham-Van-Diep, P. Keeley, E. P. Muntz, and D. P. Weaver: in *Rarefied Gas Dynamics* (J. Harvey and G. Lord), (Oxford U.P., Oxford, 1995) 715–721.

[6] Y. Sone, Y. Waniguchi, and K. Aoki: *Phys. Fluids* **8** (1996) 2227–2235.

[7] K. Aoki, Y. Sone, S. Takata, K. Takahashi, and G. A. Bird: in *Rarefied Gas Dynamics* (T. J. Bartel and M. A. Gallis), (AIP, New York, 2001) 940–947.

[8] K. Aoki and P. Degond: *Multiscale Model. Simul.* **1** (2003) 304–334.

[9] C. J. T. Laneryd, K. Aoki, P. Degond, and L. Mieussens: in *Rarefied Gas Dynamics* (M. S. Ivanov and A. K. Rebrov), (Severian Branch of the Russian Academy of Scineces, Novosibirsk, 2007) 1111–1116.

[10] Y. Sone and H. Sugimoto: in *Rarefied Gas Dynamics* (A. Ketsdever and E. P. Muntz), (AIP, New York, 2003) 1041–1048; H. Sugimoto and Y. Sone: J. Vac. Soc. Jpn. **45** (2002) 138–141.

[11] S. Takata, H. Sugimoto, and S. Kosuge: *Eur. J. Mech. B/Fluids* **26** (2007) 155-181.

[12] H. Sugimoto and Y. Sone: in *Rarefied Gas Dynamics*, (A. Ketsdever and E. P. Muntz), (AIP, New York, 2005) 168–173;

[13] H. Sugimoto: J. Vac. Soc. Jpn, **49** (2006) 481–487.

[14] H. Sugimoto, S. Takata, and S. Kosuge: in *Rarefied Gas Dynamics* (M. S. Ivanov and A. K. Rebrov), (Severian Branch of the Russian Academy of Scineces, Novosibirsk, 2007) 1158–1163.

[15] Y. Sone and M. Yoshimoto: *Phys. Fluids* **19** (1997) 3530-3534.

[16] K. Aoki, Y. Sone, and N. Masukawa: in *Rarefied Gas Dynamics* (J. Harvey and G. Lord), (Oxford U.P., Oxford, 1995) 35–41.

[17] Y. Sone: *Molecular Gas Dynamics*, (Birkh auser, Boston, 2007).

[18] G. A. Bird: *Molecular Gas Dynamics and the Direct Simulation of Gas Flows* (Clarendon, Oxford,1994).